Spatiotemporal dynamics of ultrarelativistic beam-plasma instabilities

P. San Miguel Claveria,[1,*] X. Davoine,[2,3] J. R. Peterson,[4,5] M. Gilljohann,[1] I. Andriyash,[1] R. Ariniello,[6] C. Clarke,[4] H. Ekerfelt,[4] C. Emma,[4] J. Faure,[2,3] S. Gessner,[4] M. J. Hogan,[4] C. Joshi,[7] C. H. Keitel,[8] A. Knetsch,[1] O. Kononenko,[1] M. Litos,[6] Y. Mankovska,[1] K. Marsh,[7] A. Matheron,[1] Z. Nie,[7] B. O'Shea,[4] D. Storey,[4] N. Vafaei-Najafabadi,[9] Y. Wu,[7] X. Xu,[4] J. Yan,[9] C. Zhang,[7] M. Tamburini,[8] F. Fiuza,[4] L. Gremillet,[2,3,†] and S. Corde[1,‡]

[1]*LOA, ENSTA Paris, CNRS, Ecole Polytechnique, Institut Polytechnique de Paris, 91762 Palaiseau, France*

[2]*CEA, DAM, DIF, 91297 Arpajon, France*

[3]*Université Paris-Saclay, CEA, LMCE, 91680 Bruyères-le-Châtel, France*

[4]*SLAC National Accelerator Laboratory, Menlo Park, California 94025, USA*

[5]*Physics Department, Stanford University, Stanford, California 94305, USA*

[6]*Department of Physics, University of Colorado Boulder, Center for Integrated Plasma Studies, Boulder, Colorado 80309, USA*

[7]*University of California Los Angeles, Los Angeles, California 90095, USA*

[8]*Max-Planck-Institut für Kernphysik, Saupfercheckweg 1, D-69117 Heidelberg, Germany*

[9]*Stony Brook University, Stony Brook, New York 11794, USA*

(Received 27 June 2021; accepted 28 February 2022; published 2 May 2022)

An electron or electron-positron beam streaming through a plasma is notoriously prone to microinstabilities. For a dilute ultrarelativistic infinite beam, the dominant instability is a mixed mode between longitudinal two-stream and transverse filamentation modes, with a phase velocity oblique to the beam velocity. A spatiotemporal theory describing the linear growth of this oblique mixed instability is proposed which predicts that spatiotemporal effects generally prevail for finite-length beams, leading to a significantly slower instability evolution than in the usually assumed purely temporal regime. These results are accurately supported by particle-in-cell (PIC) simulations. Furthermore, we show that the self-focusing dynamics caused by the plasma wakefields driven by finite-width beams can compete with the oblique instability. Analyzed through PIC simulations, the interplay of these two processes in realistic systems bears important implications for upcoming accelerator experiments on ultrarelativistic beam-plasma interactions.

DOI: 10.1103/PhysRevResearch.4.023085

A large number of astrophysical and laboratory systems involve the collective interaction between beams of relativistic charged particles and plasmas. In many cases, this interaction is governed by plasma microinstabilities, which lead to electrostatic and electromagnetic fluctuations growing at kinetic scales, and mediating most of the energy and momentum transfers between the beam and plasma particles [1,2].

In astrophysics these instabilities are thought to dissipate into heat or radiation the kinetic energy of relativistic outflows from various powerful sources (e.g., pulsar wind nebulae, neutron star mergers, active galactic nuclei). Notably, as a result of their nonlinear evolution [3], they can spawn relativistic collisionless shock waves [4] which, in turn, are believed to generate the most energetic particles and radiations in the universe [5], including the electromagnetic counterpart of gravitational wave sources [6]. Beam-plasma instabilities therefore lie at the heart of the fast-emerging field of multi-messenger astrophysics [7]. Another topic of active current research is their possibly crucial role in shaping the GeV photon emission from blazars, the microphysics of which remaining little understood [8].

Beyond their fundamental and astrophysical significance, these instabilities have a prominent place in experimental concepts utilizing relativistic beam-plasma interactions, such as staging of laser (LWFA) and plasma wakefield acceleration (PWFA) [9], or laser-driven ion acceleration [10,11], against which they act detrimentally. Lately it has also been proposed to harness them as a novel channel of γ-ray radiation [12]. Now progress in particle accelerators makes it possible to envision probing these plasma processes in the laboratory [13]. In particular, extreme beam parameters, with Lorentz factors $\gamma_b > 10^4$ and densities $n_b = 10^{18} - 10^{20}\,\mathrm{cm}^{-3}$, will soon be available at the new Facility for Advanced Accelerator Tests II (FACET-II) [14]. This will open unprecedented opportunities to investigate, under various plasma conditions and in a very controlled way, the effects of microinstabilities on beam propagation in the ultrarelativistic regime.

The microinstabilities arising in a relativistic beam-plasma system are usually classified into three types: the longitudinal two-stream instability (TSI), the transverse current

*pablo.san-miguel-claveria@polytechnique.edu
†laurent.gremillet@cea.fr
‡sebastien.corde@polytechnique.edu

filamentation instability (CFI), and the mixed mode, or oblique two-stream instability (OTSI) [2,15]. While several modes can develop simultaneously from thermal noise or beam-induced perturbations, a specific instability class generally dominates the early beam-plasma interaction. A fully kinetic theory exists which describes the linear phase of the instability for unbounded (i.e., infinite) beam-plasma systems, allowing the dominant mode to be predicted for a given set of beam-plasma parameters [2,16]. A key finding is the dominance of the mixed mode over CFI and TSI in the case of ultrarelativistic ($\gamma_b \gg 1$) and dilute ($\alpha \equiv n_b/n_p \ll 1$, where n_p is the electron plasma density) beams. This leads to density and field modulations with a longitudinal wave number $k_x \simeq c/\omega_p \equiv k_p$ and a transverse wave number $k_\perp \gtrsim k_p$, growing at a maximum rate

$$\Gamma_{\rm OTSI} = \frac{\sqrt{3}}{2^{4/3}} \left(\frac{1}{\gamma_b} \frac{n_b}{n_p} \frac{k_\perp^2}{k_p^2 + k_\perp^2} \right)^{1/3} \omega_p, \qquad (1)$$

where ω_p is the background plasma frequency and n_b is the sum of the number densities $n_{b\pm}$ of the beam electrons and positrons (if any). Still, this temporal theory cannot be directly applied to the finite-size beams or plasma boundaries involved in realistic settings, such as future high-energy accelerator experiments. The first attempts to account for inhomogeneity effects on linear beam-plasma instabilities concerned the TSI [17,18], revealing its pulse-shaped profile in the case of localized initial disturbances. Recently a model of the CFI excited by a longitudinally semi-infinite beam was proposed [19], showing that for moderate Lorentz factors ($\gamma_b \leqslant 10$), spatiotemporal effects are present at the beam head. Interestingly, this model predicts spatiotemporal effects to vanish in the ultrarelativistic limit.

For oblique modes, thought to dominate for $\gamma_b \gg 1$ and $\alpha \ll 1$, no spatiotemporal theory exists [20]. Yet, from the above previous works and related studies of laser-plasma [21,22] or beam-plasma [23,24] instabilities, one may expect finite beam dimensions—or, more generally, boundaries in the beam-plasma system—to strongly impact the dynamics of the oblique modes.

In this article we address two phenomena arising when a relativistic beam of finite spatial extent is considered in a beam-plasma system subject to streaming instabilities. First, we develop a spatiotemporal theory for the evolution of the OTSI, highlighting its spatiotemporal nature and resulting slower dynamics when a finite beam length is considered. Second, we show that the interplay of beam-plasma instabilities and the wakefield that is excited by a beam of finite length and width conveys constraints on the system parameters for the instabilities to dominate the interaction. These results are particularly relevant to future accelerator experiments aiming to explore ultrarelativistic beam-plasma instabilities and their radiative by-products [12]. We start by presenting the results of two-dimensional (2D) PIC CALDER [25] simulations of an ultrarelativistic ($\gamma_b = 2 \times 10^4$), low-density ($\alpha = 0.03$) electron beam interacting with a uniform electron-proton plasma. The mesh size was set to $(\Delta x, \Delta y) = (0.042, 0.084) k_p^{-1}$, the time step was $\Delta t = 0.041 \omega_p^{-1}$, and 100 macroparticles per cell were used for each species (beam electrons, plasma electrons, and ions). The beam profile was taken to be Gaussian

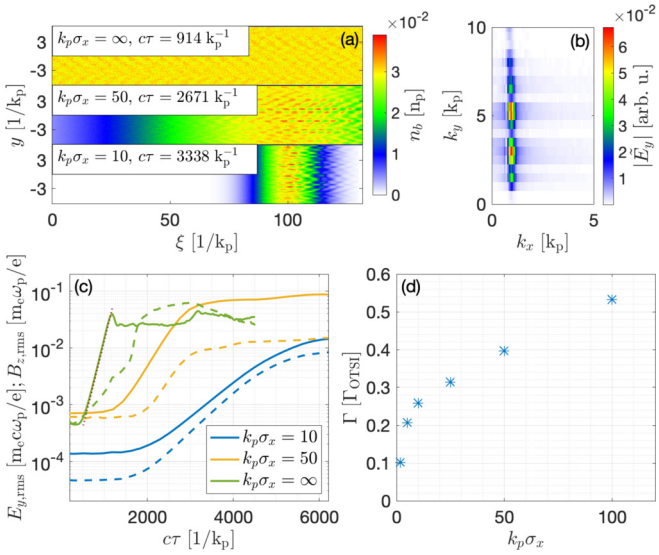

FIG. 1. Simulated instability dynamics for ultrarelativistic ($\gamma_b = 2 \times 10^4$), dilute ($\alpha = 0.03$) electron beams of various normalized lengths ($k_p\sigma_x$). (a) Snapshots of the beam density profile in the comoving coordinates $(\xi, \tau) = (v_b t - x, t)$ for different beam lengths. (b) 2D Fourier spectrum of the E_y field fluctuations at $c\tau = 3338 k_p^{-1}$ for $k_p\sigma_x = 10$. (c) Transverse electric field $E_{y,\mathrm{rms}} = \langle E_y^2 \rangle^{1/2}$ (solid line) and magnetic field $B_{z,\mathrm{rms}} = \langle B_z^2 \rangle^{1/2}$ (dashed line) averaged over $\xi \in [\xi_{\mathrm{peak}} - \sigma_x/2, \xi_{\mathrm{peak}} + \sigma_x/2]$ (ξ_{peak} the position of the beam center in the comoving coordinates) as a function of the beam propagation distance in the plasma ($c\tau$) and the beam length. The dotted line plots the theoretical growth of the OTSI, Eq. (1), in the infinite-beam case. The evaluation of the dominant $k_\perp$ in Eq. (1) is carried out using the electrostatic result $\langle E_y^2 \rangle / \langle E_x^2 \rangle \simeq (k_\perp/k_p)^2$. (d) Effective growth rate ($\Gamma/\Gamma_{\rm OTSI}$) vs $k_p\sigma_x$ within the central slice of the beam (see text for details).

in the longitudinal (x) direction with a rms length of σ_x and uniform in the transverse (y) direction. Unless otherwise mentioned, the boundary conditions were absorbing along x and periodic along y, for both the fields and particles.

Figure 1(a) illustrates the chevron-shaped pattern imprinted on the beam density profile by the OTSI in the cases of finite and infinite (i.e., with periodic boundary conditions along x) beam lengths. Galilean beam-frame coordinates $(\xi, \tau) = (v_b t - x, t)$ are used here, and the beam density maximum is located at $\xi \simeq 100 k_p^{-1}$ for $k_p\sigma_x \in (10, 50)$. While the density modulations are uniform in the infinite-beam case, they exhibit a clear spatial growth for finite σ_x. Figure 1(b) shows the 2D Fourier spectrum of the transverse E_y fluctuations within a slice around the beam maximum for $k_p\sigma_x = 10$ [i.e., corresponding to the bottom plot of Fig. 1(a)] and $c\tau = 3338 k_p^{-1}$. A narrow continuum of modes located at $k_x \simeq k_p$ and $k_\perp \gtrsim k_p$ are excited, a characteristic feature of the OTSI [2].

The evolution of the rms amplitude of the transverse E_y and B_z fields during the beam propagation in the plasma is presented in Fig. 1(c). In all cases considered, E_y prevails over B_z, as is expected for the OTSI [26]. For an infinite beam, good agreement is found with the temporal growth rate given by Eq. (1). By contrast, we observe a slowdown in the E_y field growth as the beam length is decreased from $k_p\sigma_x = 50$ to

$k_p\sigma_x = 10$. To get a spatially resolved estimate of the effective OTSI growth rate in the finite-σ_x simulations, we have fitted to an exponential the temporal evolution of the E_y energy contained in the "oblique" spectral range $0.8 \leqslant k_x/k_p \leqslant 5$ and $0.8 \leqslant k_\perp/k_p \leqslant 10$ and normalized the resulting growth rate, Γ, to $\Gamma_{\rm OTSI}$. In doing so, we have evaluated $k_\perp$ from the ratio of the E_y and E_x spectral energies integrated in the above k range. Figure 1(d) displays the results of this procedure as a function of $k_p\sigma_x$. It is clearly seen that, even for $k_p\sigma_x \gg 1$, the effective growth rate is substantially smaller than is predicted for an unbounded system.

To understand the simulation results, we have developed a spatiotemporal model describing the growth of linear electrostatic oblique modes in a transversely homogeneous, relativistic beam-plasma system in the presence of immobile ions. The analysis is restricted to a 2D (x, y) geometry, but it can be readily generalized to three dimensions (3D). Let us denote the equilibrium quantities with a superscript $^{(0)}$ and perturbed variables with a superscript $^{(1)}$. Coupling the linearized, cold-fluid momentum and continuity equations for the beam (subscript $_b$) and plasma (subscript $_p$) electrons results in

$$(\partial_t + v_{b0}\partial_x)^2 n_b^{(1)} = n_{b0}\left(\gamma_{b0}^{-1}\partial_y^2 - \gamma_{b0}^{-3}\partial_x^2\right)\phi^{(1)}, \tag{2}$$

$$\partial_t^2 n_p^{(1)} = n_{p0}\left(\partial_y^2 - \partial_x^2\right)\phi^{(1)}. \tag{3}$$

Next, using the linearized Poisson equation to express the perturbed electrostatic potential $\phi^{(1)}$ in terms of $n_p^{(1)}$ and $n_b^{(1)}$, one can obtain, after some algebra, the following differential equation for the perturbed plasma density:

$$\left[\left(\partial_x^2 + \partial_y^2\right)(\partial_t + v_{b0}\partial_x)^2\left(\partial_t^2 + n_{p0}\right) + \gamma_{b0}^{-1} n_{b0}\partial_y^2\partial_t^2\right] n_p^{(1)} = 0, \tag{4}$$

where the beam Lorentz factor has been supposed large enough that $\partial_y^2 \gg \gamma_{b0}^{-2}\partial_x^2$. We now adopt the comoving coordinates defined above to express the plasma density perturbation as $n_p^{(1)} = \delta n_p(\tau, \xi)e^{-ik_p\xi + ik_\perp y}$, where $\delta n_p(\tau, \xi)$ represents a slowly varying envelope. Writing Eq. (4) in terms of the comoving variables and assuming that $k_p \gg v_{b0}^{-1}\partial_\tau, \partial_\xi$, one can derive the following approximate differential equation satisfied by δn_p:

$$\left(\partial_\tau^3 + v_b\partial_\tau^2\partial_\xi + \frac{8i}{3^{3/2}}\Gamma_{\rm OTSI}^3\right)\delta n_p = 0. \tag{5}$$

This equation can be solved analytically for a semi-infinite electron (or electron-positron) beam whose front edge is located at $\xi = 0$ (see Supplemental Material [27]). Following Refs. [19,21], we assume an initial noise source throughout the beam, i.e., $\delta n_p(\tau = 0, \xi) = \delta n_p(\tau, \xi = 0) = S$ and $\partial_\tau \delta n_p(\tau = 0, \xi) = \partial_\tau^2 \delta n_p(\tau = 0, \xi) = 0$, where S is some amplitude parameter. Such conditions mainly apply to a situation where the beam is created within the plasma or penetrates a plasma with a long density ramp. An asymptotic solution to Eq. (5) can then be obtained in the $\tau \to \infty$ limit using a double Laplace transform and a saddle-point expansion [27]. When $\xi \ll v_b\tau$, one finds

$$\delta n_p(\tau, \xi) \simeq \frac{S}{\sqrt{6\pi}}\left(\frac{3\sqrt{3}v_b}{16\Gamma_{\rm OTSI}^3\,\xi\,\tau^2}\right)^{1/6} \times \exp\left[\frac{\sqrt{3}}{2^{2/3}}(\sqrt{3} + i)\Gamma_{\rm OTSI}\left(\frac{\xi}{v_b}\right)^{1/3}\tau^{2/3} - i\frac{\pi}{12}\right]. \tag{6}$$

This solution, similar to the asymptotic impulse solution of the TSI [18], demonstrates the spatiotemporal character of the oblique instability. Different longitudinal ξ slices of the beam experience different temporal evolutions, the fastest growth being present at the rear of the beam, as might be intuitively surmised. The same leading exponential term is found for an initial noise source localized at the beam front, as expected when the beam enters a sharp vacuum-plasma boundary [27].

Further away from the beam front, i.e., for $\xi \geqslant v_b\tau$, the solution asymptotically evolves as

$$\delta n_p(\tau, \xi) \simeq \frac{S}{3}\exp\left[\left(1 + \frac{i}{\sqrt{3}}\right)\Gamma_{\rm OTSI}\,\tau\right], \tag{7}$$

which exhibits a purely temporal growth at the rate given by Eq. (1). In fact, the same exponential behavior sets in for $\xi \gtrsim v_b\tau/3$ but with a smaller prefactor [27]. In the comoving coordinates, the region of purely temporal growth recedes from the front to the rear of the beam at a velocity of $\sim v_b/3$. Therefore, at a location ξ behind the beam front, the instability initially grows in a purely temporal manner at a rate $\Gamma_{\rm OTSI}$, up to $\tau \simeq 3\xi v_b^{-1}$, after which spatiotemporal effects turn prominent and result in a slower growth. The same reasoning applied to a finite beam length σ_x implies that for $\sigma_x \ll v_b\Gamma_{\rm OTSI}^{-1}$, the instability is essentially of spatiotemporal nature. The latter condition holds in particular for the short ultrarelativistic bunches produced in particle accelerators.

To support this analysis, we carried out 2D PIC simulations with a steplike beam profile. A neutral electron-positron (e^-e^+) pair beam was employed in order to avoid plasma wakefield excitation and minimize initial noise, thus enabling accurate comparison with the model (yet similar results were obtained with an electron beam [27]). To reproduce even more closely the model assumptions, the beam entering the plasma was propagated ballistically until being completely immersed, and then (at $t = 0$) let to evolve freely. We used beam-plasma parameters relevant to FACET-II: $\gamma_b = 2 \times 10^4$, $\alpha = (n_{b-} + n_{b+})/n_p = 0.06$ ($n_{b\pm}$ is the equal density of the beam electrons and positrons), and $n_p = 10^{20}\,{\rm cm}^{-3}$. The simulation (moving) window covered the longitudinal range $-10 \leqslant \xi \leqslant \xi_{\rm max} = 150\,\mu$m (i.e., $-19 \leqslant k_p\xi \leqslant 282$), the beam front being placed at $\xi = 0$. For these parameters one finds $\xi_{\rm max} < v_b\Gamma_{\rm OTSI}^{-1}$, and hence the instability should evolve in a spatiotemporal manner.

Figure 2(a) displays (in solid curves) the spectral amplitude $|\widetilde{E}_y(k_x, k_\perp)|$ of the dominant oblique mode (at $k_x = k_p$ and $k_\perp \simeq 3k_p$) along the beam at different propagation distances $c\tau$, and in Fig. 2(b) the same quantity is plotted as a function of $c\tau$ for different positions ξ. Both figures show very good agreement with the predicted spatiotemporal evolution $\propto \exp[(3/2^{2/3})\Gamma_{\rm OTSI}(\xi/c)^{1/3}\tau^{2/3}]$ of the instability (dashed lines).

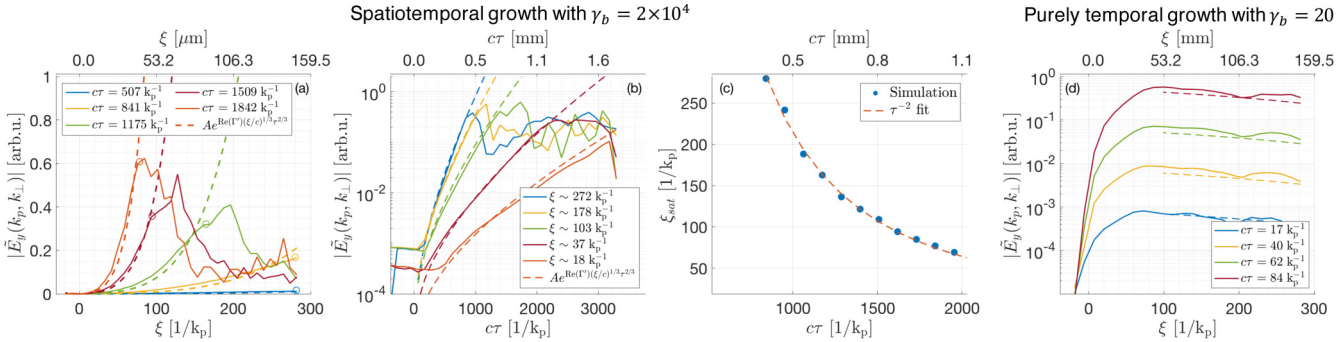

FIG. 2. 2D PIC simulations of the OTSI induced by a steplike e^-e^+ pair beam and comparison with linear theory in the spatiotemporal regime for $\gamma_b = 2 \times 10^4$ (a)–(c) and the temporal regime for $\gamma_b = 20$ (d). (a), (d) Spectral amplitude $|\widetilde{E}_y(k_x, k_\perp)|$ of the dominant oblique mode ($k_x = k_p, k_\perp \simeq 3k_p$) as a function of ξ for different propagation distances $c\tau$. (b) Same quantity but as a function of $c\tau$ for different beam slices ξ. In (a) and (b), the simulation data (solid lines) is fitted to the theoretical law $A\exp[(3/2^{2/3})\Gamma_{\rm OTSI}(\xi/c)^{1/3}\tau^{2/3}]$ for $\xi \leqslant \xi_{\rm sat}$ (dashed lines). (c) Saturation position $\xi_{\rm sat}$ [also shown in (a) as circles] vs $c\tau$ (filled circles), compared with the theoretical expectation $\xi_{\rm sat} \propto \tau^{-2}$ (red dashed line). Dashed lines in (d) plot the theoretical temporal growth of $|\widetilde{E}_y(k_p, 3k_p)|$ at different times $c\tau \geqslant 17{\rm k}_{\rm p}^{-1}$.

For large enough propagation distances ($c\tau \gtrsim 1000k_p^{-1}$), the simulation curves in Fig. 2(a) peak at some position ξ, beyond which they rapidly decay. This behavior is due to the nonlinear saturation of the OTSI [8,28]. The saturation mechanisms involved in the ultrarelativistic regime will be studied in a separate paper, yet one can exploit here their observed weak spatial dependence to further validate the theory. Indeed, assuming that the instability ceases when a certain field level is reached, the saturation position, $\xi_{\rm sat}$, should vary with τ as $\xi_{\rm sat} \propto \tau^{-2}$. This prediction matches well with the simulation results of Fig. 2(c), which plots $\xi_{\rm sat}$ vs τ.

Finally, to confirm the existence of a purely temporal regime, we repeated the same simulation but with a lower beam Lorentz factor ($\gamma_b = 20$), so that $\xi_{\rm max} > v_b\Gamma_{\rm OTSI}^{-1}$. Figure 2(d) shows that the instability then grows at a rate that is essentially independent of the beam slice $\xi > 50\,\mu$m. This nicely agrees with Eq. (7), as shown by the dashed lines representing the predicted amplification of the initial (recorded at $c\tau = 14k_p^{-1}$) ξ-dependent fluctuations.

Another important finite-size effect is the excitation of plasma wakefields by non-neutral beams with relatively small transverse width (σ_r). These fields act back on the beam to pinch it, which reinforces them and causes the beam to self-focus as it further propagates through the plasma [29]. The timescale of beam self-focusing can be estimated by the inverse betatron frequency $\omega_\beta^{-1} = \sqrt{\gamma_b m_e/\partial_r W_\perp}$, where $W_\perp$ is the amplitude of the transverse wakefield [30]. If this timescale is smaller than the effective growth time of the dominant oblique instability [i.e., lengthened by spatiotemporal effects, see Fig. 1(d)], the beam can shrink into a narrow and dense filament expelling the plasma electrons away from it, hence quenching the instability. For a beam with fixed charge and length, changing its transverse width affects both processes similarly and so barely modifies their interplay. By contrast, raising the plasma density tends to favor the instability over the beam self-focusing.

We ran additional 2D PIC simulations to examine the interplay of the beam self-focusing and beam-plasma instability depending on the plasma density. Potential effects arising in a 3D geometry are discussed in the Supplemental Material [27]. We considered a FACET-II-like electron beam (10 GeV, 2 nC, $\sigma_x = 5\,\mu$m, $\sigma_r = 10\,\mu$m, peak density $n_b \simeq 1.5 \times 10^{18}\,{\rm cm}^{-3}$, normalized emittance $\epsilon_n = 3\,$mm mrad) injected through a uniform plasma of different densities. Each simulation was repeated with a transversely infinite (periodic) beam to suppress the effects of plasma wakefields and beam self-focusing. Comparing ω_β^{-1} to the timescale of the spatiotemporal OTSI with the above parameters, one finds that beam self-focusing should dominate for $n_p \lesssim 10^{19}\,{\rm cm}^{-3}$ [27]. This prediction is confirmed by the simulation results depicted in Fig. 3. At $n_p = 10^{19}\,{\rm cm}^{-3}$ [Figs. 3(a)–3(c)], the transverse wakefield starts focusing the finite-width beam [see its rotation in the transverse phase space in the inset of Fig. 3(a)] before the OTSI can impart significant modulations on the beam profile. This leads the whole beam to collapse into a narrow filament [Figs. 3(b) and 3(c)], hence inhibiting the OTSI, in stark contrast with the equivalent infinite-beam simulation [Figs. 3(d)–3(f)]. At $n_p = 2.5 \times 10^{19}\,{\rm cm}^{-3}$ [Figs. 3(g)–3(i)], the self-focusing dynamics is slower, and so the competition between the two processes is more balanced. Still, although the OTSI-driven modulations have time to grow, a compressed filament eventually forms at the beam center [Fig. 3(i)], which is absent for an infinite beam width [Fig. 3(l)]. Finally, when further increasing the plasma density to $n_p = 5 \times 10^{19}\,{\rm cm}^{-3}$ [Figs. 3(m)–3(r)], the system dynamics is clearly governed by the OTSI, and, as expected, no significant difference arises when changing from a finite to an infinite beam width.

In conclusion, we have conducted the first spatiotemporal analysis of the oblique two-stream instability triggered by finite-size particle beams. For ultrarelativistic, short-duration bunches, such as delivered by state-of-the-art particle accelerators, we have shown analytically that in terms of the comoving coordinates (τ, ξ), the instability mainly evolves as a function of $(\xi/v_b)^{1/3}\tau^{2/3}$. It develops from the head to the tail of the beam and, within a fixed beam slice, more slowly than in unbounded geometry. Close agreement has been found between the theory and PIC simulations in several beam-plasma setups. Furthermore, when realistic finite-width electron beams are considered, self-focusing induced by

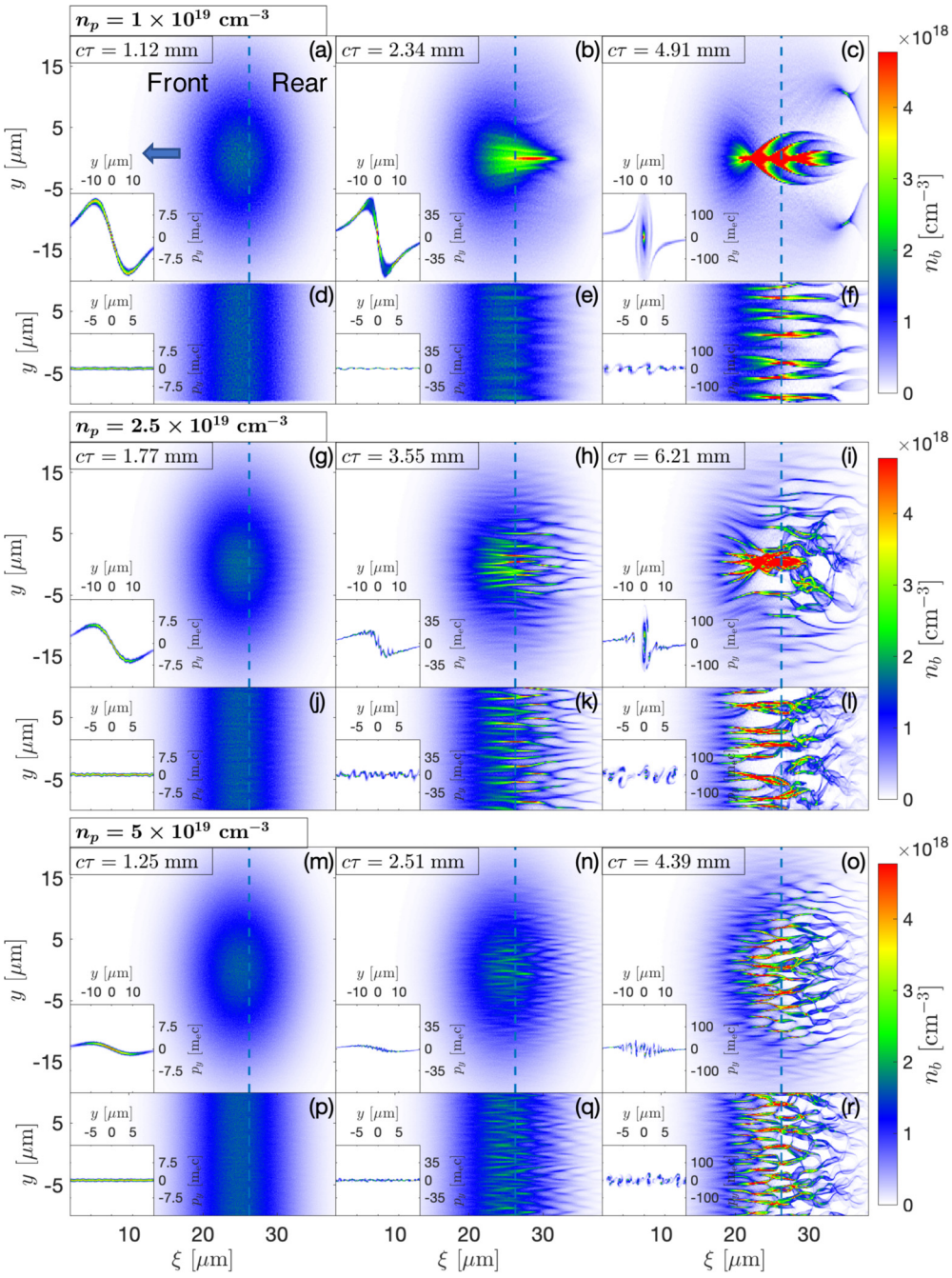

FIG. 3. Simulated electron-beam-density maps at different propagation distances in a uniform plasma of density $n_p = 1 \times 10^{19}\,\mathrm{cm}^{-3}$ (a)–(f), $2.5 \times 10^{19}\,\mathrm{cm}^{-3}$ (g)–(l), and $5 \times 10^{19}\,\mathrm{cm}^{-3}$ (m)–(r). The transverse beam profile is taken to be either finite with $\sigma_r = 10\,\mu$m rms width [(a)–(c), (g)–(i), and (m)–(o)] or infinite, i.e., with transverse periodic boundary conditions [(d)–(f), (j)–(l), and (p)–(r)]. In all cases, the beam has a 10-GeV energy ($\gamma_b = 2 \times 10^4$), a Gaussian longitudinal profile with $\sigma_x = 5\,\mu$m rms length, a transverse normalized emittance $\epsilon_n = 3$ mm mrad, and a peak density $n_b \simeq 1.5 \times 10^{18}\,\mathrm{cm}^{-3}$ [i.e., $\alpha \simeq 0.15$ for (a)–(f), $\alpha \simeq 0.06$ for (g)–(l), and $\alpha \simeq 0.03$ for (m)–(r)], which would correspond to a total beam charge of 2 nC in 3D. The insets show the transverse beam phase space along the slices indicated by the dashed blue lines.

plasma wakefields may hinder the instability growth and thus dominate the beam dynamics. Neutral pair beams, though, can circumvent the limitation placed by wakefields and facilitate laboratory investigations of ultrarelativistic streaming instabilities. These results are critical to guide and interpret future experiments on high-energy beam-plasma interactions and their envisioned applications, such as the development of instability-based light sources.

This work was performed within the framework of the E-305 Collaboration. E-305 is a SLAC experiment which aims at the study of astrophysically relevant beam-plasma

instabilities and at the generation of bright γ rays. The work at CEA and LOA was supported by the ANR (UnRIP project, Grant No. ANR-20-CE30-0030). The work at LOA was also supported by the European Research Council (ERC) under the European Union's Horizon 2020 Research and Innovation Programme (M-PAC project, Grant Agreement No. 715807). We acknowledge GENCI-TGCC for granting us access to the supercomputer IRENE under Grants No. 2019-A0060510786, No. 2020-A0080510786, and No. 2021-A0100510786 to run PIC simulations. J. R. Peterson was supported by a DOE NNSA LRGF fellowship under Grant No. DE-NA0003960. The work at SLAC was supported by the U.S. DOE FES Grant No. FWP100331 and DOE Contract No. DE-AC02-76SF00515. UCLA is supported by the U.S. Department of Energy through Grant No. DE-SC001006 and the NSF through Grant No. 2003354.

[1] R. N. Sudan, Collective beam-plasma interaction, in *Handbook of Plasma Physics*, edited by M. N. Rosenbluth and R. Z. Sagdeev (North-Holland Physics Publishing, Amsterdam, 1984), Vol. 2, Chap. 6.3, pp. 337–382.

[2] A. Bret, L. Gremillet, and M. E. Dieckmann, Multidimensional electron beam-plasma instabilities in the relativistic regime, Phys. Plasmas **17**, 120501 (2010).

[3] A. Bret, A. Stockem, F. Fiuza, C. Ruyer, L. Gremillet, R. Narayan, and L. O. Silva, Collisionless shock formation, spontaneous electromagnetic fluctuations, and streaming instabilities, Phys. Plasmas **20**, 042102 (2013).

[4] A. Spitkovsky, Particle acceleration in relativistic collisionless shocks: Fermi process at last? Astrophys. J. **682**, L5 (2008); M. Lemoine, L. Gremillet, G. Pelletier, and A. Vanthieghem, Physics of Weibel-Mediated Relativistic Collisionless Shocks, Phys. Rev. Lett. **123**, 035101 (2019).

[5] R. Blandford and D. Eichler, Particle acceleration at astrophysical shocks: A theory of cosmic ray origin, Phys. Rep. **154**, 1 (1987); A. M. Bykov and R. A. Treumann, Fundamentals of collisionless shocks for astrophysical application, 2. Relativistic shocks, Astron. Astrophys. Rev. **19**, 42 (2011).

[6] B. P. Abbott *et al.*, Multi-messenger observations of a binary neutron star merger, Astrophys. J. **848**, L12 (2017).

[7] P. Mészáros, D. B. Fox, C. Hanna, and K. Murase, Multi-messenger astrophysics, Nat. Rev. Phys. **1**, 585 (2019).

[8] A. E. Broderick, P. Chang, and C. Pfrommer, The cosmological impact of luminous TeV Blazars. I. Implications of plasma instabilities for the intergalactic magnetic field and extragalactic gamma-ray background, Astrophys. J. **752**, 22 (2012); L. Sironi and D. Giannios, Relativistic pair beams from TeV blazars: A source of reprocessed GeV emission rather than intergalactic heating, *ibid.* **787**, 49 (2014); P. Chang, A. E. Broderick, C. Pfrommer, E. Puchwein, A. Lamberts, M. Shalaby, and G. Vasil, The linear instability of dilute ultrarelativistic $e^{\pm}$ pair beams, *ibid.* **833**, 118 (2016).

[9] G. Raj, O. Kononenko, M. F. Gilljohann, A. Doche, X. Davoine, C. Caizergues, Y.-Y. Chang, J. P. Couperus Cabadağ, A. Debus, H. Ding, M. Förster, J.-P. Goddet, T. Heinemann, T. Kluge, T. Kurz, R. Pausch, P. Rousseau, P. San Miguel Claveria, S. Schöbel, A. Siciak *et al.*, Probing ultrafast magnetic-field generation by current filamentation instability in femtosecond relativistic laser-matter interactions, Phys. Rev. Research **2**, 023123 (2020).

[10] J. Fuchs, T. E. Cowan, P. Audebert, H. Ruhl, L. Gremillet, A. Kemp, M. Allen, A. Blazevic, J.-C. Gauthier, M. Geissel, M. Hegelich, S. Karsch, P. Parks, M. Roth, Y. Sentoku, R. Stephens, and E. M. Campbell, Spatial Uniformity of Laser-Accelerated Ultrahigh-Current MeV Electron Propagation in Metals and Insulators, Phys. Rev. Lett. **91**, 255002 (2003).

[11] S. Göde, C. Rödel, K. Zeil, R. Mishra, M. Gauthier, F.-E. Brack, T. Kluge, M. J. MacDonald, J. Metzkes, L. Obst, M. Rehwald, C. Ruyer, H.-P. Schlenvoigt, W. Schumaker, P. Sommer, T. E. Cowan, U. Schramm, S. Glenzer, and F. Fiuza, Relativistic Electron Streaming Instabilities Modulate Proton Beams Accelerated in Laser-Plasma Interactions, Phys. Rev. Lett. **118**, 194801 (2017).

[12] A. Benedetti, M. Tamburini, and C. H. Keitel, Giant collimated gamma-ray flashes, Nat. Photonics **12**, 319 (2018).

[13] B. Allen, V. Yakimenko, M. Babzien, M. Fedurin, K. Kusche, and P. Muggli, Experimental Study of Current Filamentation Instability, Phys. Rev. Lett. **109**, 185007 (2012).

[14] V. Yakimenko, L. Alsberg, E. Bong, G. Bouchard, C. Clarke, C. Emma, S. Green, C. Hast, M. J. Hogan, J. Seabury, N. Lipkowitz, B. O'Shea, D. Storey, G. White, and G. Yocky, FACET-II facility for advanced accelerator experimental tests, Phys. Rev. Accel. Beams **22**, 101301 (2019).

[15] M. Lemoine and G. Pelletier, On electromagnetic instabilities at ultra-relativistic shock waves, MNRAS **402**, 321 (2010).

[16] A. Bret, L. Gremillet, D. Bénisti, and E. Lefebvre, Exact Relativistic Kinetic Theory of an Electron-Beam Plasma System: Hierarchy of the Competing Modes in the System-Parameter Space, Phys. Rev. Lett. **100**, 205008 (2008).

[17] A. Bers, Space-time evolution of plasma instabilities - Absolute and convective, in *Handbook of Plasma Physics*, edited by M. N. Rosenbluth and R. Z. Sagdeev (North-Holland Physics Publishing, Amsterdam, 1983), Chap. 3.2, pp. 451–517.

[18] M. E. Jones, D. S. Lemons, and M. A. Mostrom, Space-time evolution of the beam-plasma instability, Phys. Fluids **26**, 2784 (1983).

[19] V. B. Pathak, T. Grismayer, A. Stockem, R. A. Fonseca, and L. O. Silva, Spatial-temporal evolution of the current filamentation instability, New J. Phys. **17**, 043049 (2015).

[20] N. Shukla, S. F. Martins, P. Muggli, J. Vieira, and L. O. Silva, Interaction of ultra relativistic $e^{-}e^{+}$ fireball beam with plasma, New J. Phys. **22**, 013030 (2020).

[21] C. D. Decker, W. B. Mori, T. Katsouleas, and D. E. Hinkel, Spatial temporal theory of Raman forward scattering, Phys. Plasmas **3**, 1360 (1996).

[22] C. J. McKinstrie and E. J. Turano, Spatiotemporal evolution of parametric instabilities driven by short laser pulses: One-dimensional analysis, Phys. Plasmas **3**, 4683 (1996).

[23] C. Huang, W. Lu, M. Zhou, C. E. Clayton, C. Joshi, W. B. Mori, P. Muggli, S. Deng, E. Oz, T. Katsouleas, M. J. Hogan, I. Blumenfeld, F. J. Decker, R. Ischebeck, R. H. Iverson,

N. A. Kirby, and D. Walz, Hosing Instability in the Blow-Out Regime for Plasma-Wakefield Acceleration, Phys. Rev. Lett. **99**, 255001 (2007).

[24] N. Kumar, A. Pukhov, and K. Lotov, Self-Modulation Instability of a Long Proton Bunch in Plasmas, Phys. Rev. Lett. **104**, 255003 (2010).

[25] E. Lefebvre, N. Cochet, S. Fritzler, V. Malka, M.-M. Aléonard, J.-F. Chemin, S. Darbon, L. Disdier, J. Faure, A. Fedotoff, O. Landoas, G. Malka, V. Méot, P. Morel, M. Rabec LeGloahec, A. Rouyer, C. Rubbelynck, V. Tikhonchuk, R. Wrobel, P. Audebert *et al.*, Electron and photon production from relativistic laser plasma interactions, Nucl. Fusion **43**, 629 (2003).

[26] A. Bret, L. Gremillet, and D. Bénisti, Exact relativistic kinetic theory of the full unstable spectrum of an electron-beam-plasma system with Maxwell-Jüttner distribution functions, Phys. Rev. E **81**, 036402 (2010).

[27] See Supplemental Material at http://link.aps.org/supplemental/10.1103/PhysRevResearch.4.023085 for a detailed derivation of the spatiotemporal model of the oblique instability, its comparison to electron-beam-plasma simulations, and a criterion for the dominance of the oblique instability over the beam self-focusing.

[28] L. E. Thode, Energy lost by a relativistic electron beam due to two-stream instability, Phys. Fluids **19**, 305 (1976).

[29] S. Corde, E. Adli, J. M. Allen, W. An, C. I. Clarke, B. Clausse, C. E. Clayton, J. P. Delahaye, J. Frederico, S. Gessner, S. Z. Green, M. J. Hogan, C. Joshi, M. Litos, W. Lu, K. A. Marsh, W. B. Mori, N. Vafaei-Najafabadi, D. Walz, and V. Yakimenko, High-field plasma acceleration in a high-ionization-potential gas, Nat. Commun. **7**, 11898 (2016).

[30] R. Keinigs and M. E. Jones, Two dimensional dynamics of the plasma wakefield accelerator, Phys. Fluids **30**, 252 (1987).